Synthesis, Characterization, and Properties of a Titanium(IV)-Tetrathiafulvalene-Based Complex

Jaison Casas, Stéphane Baudron, Antoine Bonnefont, Alain Chaumont, Jérôme Chauvin, Pierre Mobian, Laurent Ruhlmann

Synthesis, Characterization, and Properties of a Titanium(IV)-Tetrathiafulvalene Based Complex

Jaison Casas,[a] Stéphane A. Baudron,*[,a] Antoine Bonnefont,[b,c] Alain Chaumont,[a] Jérôme Chauvin,[d] Pierre Mobian,*[,a] Laurent Ruhlmann[b]

[a] Université de Strasbourg, CNRS, CMC UMR 7140, F-67000 Strasbourg, France. E-mail: sbaudron@unistra.fr, E-mail: mobian@unistra.fr.

[b] Université de Strasbourg, CNRS, IC UMR 7177, F-67000 Strasbourg, France. E-mail : lruhlmann@unistra.fr.

[c] LEPMI, Université Grenoble Alpes, Université Savoie Mont Blanc, CNRS, Grenoble INP, F-38000 Grenoble, France.

[d] DCM, Université Grenoble Alpes, CNRS, CS 40700, 38058 Grenoble, France.

Keywords :

Ti(IV) complex – tetrathiafulvalene – DFT – spectroelectrochemical studies – electron transfer

Abstract :

In order to deeply investigate the interaction between a tetrathiafulvalene (TTF) unit and a Ti(IV) center, a monomeric heteroleptic octahedral Ti(IV)-complex containing a diimine ligand composed of a 1,10-phenanthroline core fused with a TTF fragment (ligand **2a**) was prepared. The stable complex formulated as Ti(**1**)$_2$(**2a**), where **1** is a 2,2'-biphenolato derivative, was efficiently synthetized by following a one-step approach. This complex as well as its model species (Ti(**1**)$_2$(**2b**)), were fully characterized in solution and their solid-state structures were established *via* X-ray diffraction analysis on single crystals. DFT calculations allowed the assignment of the frontier orbitals involved in the electronic transitions characterized by UV-visible absorption spectroscopy. Electrochemical and spectroelectrochemical studies revealed that the TTF unit within Ti(**1**)$_2$(**2a**) can undergo two reversible one-electron oxidation processes, whereas a reversible one electron reduction of the Ti(IV) atom was highlighted. The photophysical measurements performed for this donor-acceptor molecular system indicated that an electron transfer process upon light excitation occurred within Ti(**1**)$_2$(**2a**).

Introduction

Owing to its well investigated semi-conductor behaviour,[1] TiO_2 elicits a major interest for applications in photocatalytic water splitting,[2] photocatalytic degradation of pollutants or solar energy conversion.[3] However, due to its high band gap (3.2 eV), the majority of TiO_2 based devices exhibit a photo-response only under UV light. Therefore, in order to develop more practical TiO_2 based photo-active materials, dye-sensitized systems have been proposed. The light–harvesting compounds explored for the functionalization of the TiO_2 surface are metal complexes or organic molecules.[4] Among the possible organic photosensitizers (PS), species incorporating a tetrathiafulvalene (TTF) core are particularly appealing owing to their remarkable redox properties (high π-electron donor ability).[5] Thus, devices where TTF derivatives and TiO_2 are associated have been engineered and some of these systems have demonstrated high photoconversion efficiencies for hydrogen production.[6] Surprisingly, discrete complexes resulting from the association of TTF derivative-based ligands and Ti-oxo clusters concern only very few reports.[7] In addition, as far as we are aware, no system combining a single Ti(IV) atom associated with one TTF unit has been designed for evaluating the donor-acceptor behaviour that could occur between these two entities.[8] Nevertheless, such type of molecular architecture is highly attractive, as it allows *a priori* to deeply investigate and facilitate the understanding of the interaction between the metallic centre and the TTF unit upon light excitation, that can then be employed to decipher phenomena observed within multinuclear and/or polymolecular aggregates.

Dyads are molecular systems composed of a donor and an acceptor fragment that exhibit photoinduced energy or charge transfer (CT) processes to mimic the events occurring in natural photosynthesis.[9] The design of these architectures relies very often on metal complexes and various types of transition metal ions belonging mainly to late elements that have been incorporated within the framework of these compounds.[10] It should be noted that titanium complexes have been extremely rarely employed to create donor-acceptor architectures.[11] In parallel, TTF units are extensively used to create dyads associated with organic acceptors (for instance fullerene,[12] perylene diimine,[13] BODIPY,[14] porphyrin,[15] or fused polyaromatic fragments[16]) or coordination complex acceptors.[17]

Thus, we wanted to combine in the same molecular system one TTF fragment and one Ti(IV) ion in order to study the interaction between these two units. Therefore, we have

undertaken in this work the preparation of a monomeric Ti(IV)-complex incorporating a TTF motif in its backbone. The design of the monomeric titanium(IV) complex-based dyad containing a TTF-based ligand reported in this study (see chart 1) relied on the ability of the proligand **1**H_2, a 2,2'-biphenol derivative, to form with Ti(IV) in the presence of nitrogen bidentate ligands, robust heteroleptic metal complexes constructed around a TiO_4N_2 framework.[18] In order to incorporate a TTF core into the framework of a Ti(IV) coordination compound, the diimine ligand **2a**, composed of a TTF unit directly fused with a 1,10-phenanthroline backbone,[19] was selected. Thus, we report herein the synthesis and the characterization of the Ti(**1**)$_2$(**2a**) complex and a model complex Ti(**1**)$_2$(**2b**) followed by the description of the electrochemical measurements and the investigation of the photophysical properties displayed by these architectures. These characterizations are next interpreted with the help of DFT calculations.

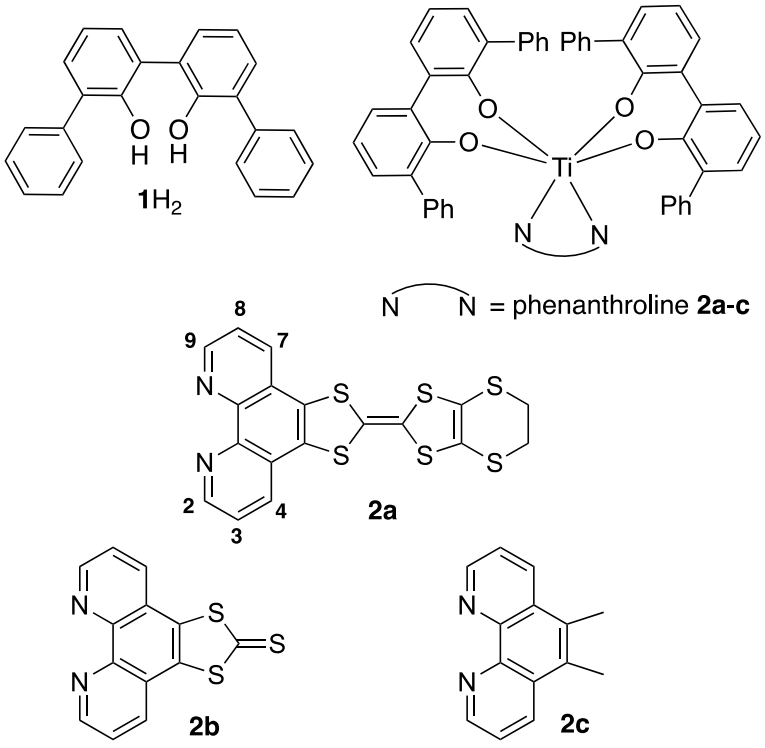

Chart 1. Proligand **1**H_2, phenanthroline **2a**-**c** and complexes Ti(**1**)$_2$(**2a**-**c**)

Results and discussion

Formation of Ti(**1**)$_2$(**2a**-**c**) complexes

The complex Ti(**1**)$_2$(**2a**) and the two model complexes, Ti(**1**)$_2$(**2b**) and the known species Ti(**1**)$_2$(**2c**) (Chart 1),[17] were prepared following a one-pot strategy as shown in eq. 1.

$$2\ \mathbf{1}H_2 + Ti(O^iPr)_4 + \mathbf{2a}\text{-}\mathbf{c} \longrightarrow Ti(\mathbf{1})_2(\mathbf{2a}\text{-}\mathbf{c}) + 4\ HO^iPr \quad \text{(eq. 1)}$$

Under inert atmosphere, the solution instantly turned from uncolored to red, upon the addition of titanium(IV) isopropoxide into a solution of one equivalent of the phenanthroline-based ligand (**2a**-**c**) and two equivalents of the proligand **1**H$_2$. Alternatively, complex Ti(**1**)$_2$(**2a**) was also synthetized starting from the Ti(**1**)$_2$(HO^{i}Pr)$_2$ precursor (eq. 2).[20] Nevertheless, this method did not permit to drastically improve the efficiency of the formation of the desired compound. It should be noted that, independently of the methodology employed, the targeted compounds were purified over silica gel chromatography, owing to their excellent robustness.

$$Ti(\mathbf{1})_2(HO^iPr)_2 + \mathbf{2a} \longrightarrow Ti(\mathbf{1})_2(\mathbf{2a}) + 2\ HO^iPr \quad \text{(eq. 2)}$$

Complexes Ti(**1**)$_2$(**2a**-**c**) were characterized by ^{1}H and ^{13}C NMR spectroscopy. The assignment of each phenanthroline proton resonance for Ti(**1**)$_2$(**2a**) was done with the help of 2D ^{1}H experiments (COSY and ROESY). The protons H$_{2,9}$, H$_{3,8}$ and H$_{4,7}$ of **2a** (see Chart 1) are shielded with a $\Delta\delta$ = 0.56, 0.53, 0.35 ppm respectively, when the diimine ligand is coordinated to Ti(IV) within Ti(**1**)$_2$(**2a**) (see SI). Altogether, these NMR analyses match with Ti(**1**)$_2$(**2a**-**c**) adopting an expected *C*$_2$ symmetry in solution. The complexes Ti(**1**)$_2$(**2a**-**c**) were also characterized by mass spectrometry. Figure 1 displays the high-resolution mass spectrum of Ti(**1**)$_2$(**2a**) showing an intense peak at *m/z* = 1167.1013. Importantly, the experimental isotopic profile matched with the superimposition of two simulated isotopic profiles, the one for [Ti(**1**)$_2$(**2a**) + H]$^+$ and the other for [Ti(**1**)$_2$(**2a**)]$^+$. The detection of a peak resulting from the superimposition of two profiles was explained by the ES source that could behave like an electrolysis cell leading to the oxidation of the TTF moiety within Ti(**1**)$_2$(**2a**) to form the [Ti(**1**)$_2$(**2a**)]$^+$ cation.[21] The peaks confirming the

presence of the desired compounds were also observed in the analysis of Ti(**1**)$_2$(**2b**-**c**) (Figure S7 in SI).

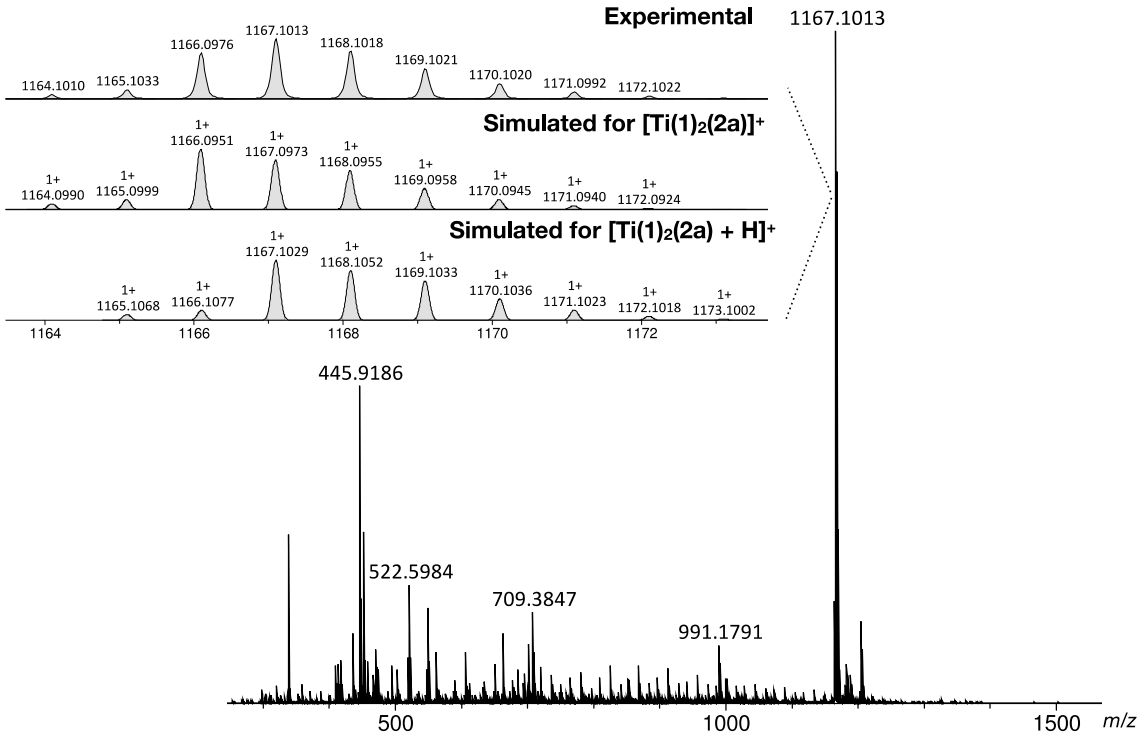

Figure 1. Mass spectrum of Ti(**1**)$_2$(**2a**) with an enlargement on the peak at *m/z* = 1167.1013 with two simulated isotopic profiles for [Ti(**1**)$_2$(**2a**) + H]$^+$ (calcd *m/z* = 1167.1029) and [Ti(**1**)$_2$(**2a**)]$^+$ (calcd *m/z* = 1166.0951).

Crystals suitable for X-ray diffraction analysis were formed from toluene for Ti(**1**)$_2$(**2a**) and from dichloromethane/diethyl ether for Ti(**1**)$_2$(**2b**) (Figure 2). Ti(**1**)$_2$(**2a**)(toluene)$_2$ and Ti(**1**)$_2$(**2b**)(CH_2Cl_2)$_2$ crystallize in the *P*2$_1$/*n* and *P*2$_1$/*c* monoclinic centrosymmetric space groups respectively. As expected, in both compounds, the coordination sphere around the titanium atom adopts a distorted octahedral geometry. The metallic center is coordinated by two chelating ligands **1** with Ti-O distances ranging between 1.8372(18) Å and 1.9038(18) Å for Ti(**1**)$_2$(**2a**) and between 1.8258(16) Å and 1.8966(16) Å for Ti(**1**)$_2$(**2b**). The two nitrogen atoms from the phenanthroline units are also coordinated to the metal cation in *cis* positions with Ti-N distances of 2.245(2) and 2.246(2) Å for the TTF-incorporating compound and of 2.2401(18) Å and 2.2456(19) Å for the model complex. The phenanthroline ligand is almost planar and π-stacking interactions between the phenyl rings and the phenanthroline unit are suggested by the short distances between the centroids of the aromatic rings (3.479 and 3.482 Å for Ti(**1**)$_2$(**2a**) and 3.584

and 3.686 Å for Ti(**1**)$_2$(**2b**)) and the parallel orientation of the phenyl ring belonging to **1** and the phenanthroline moiety of either ligand **2a** or **2b** within the complex. The unit cell contains both the Δ and Λ enantiomeric forms of the complex.

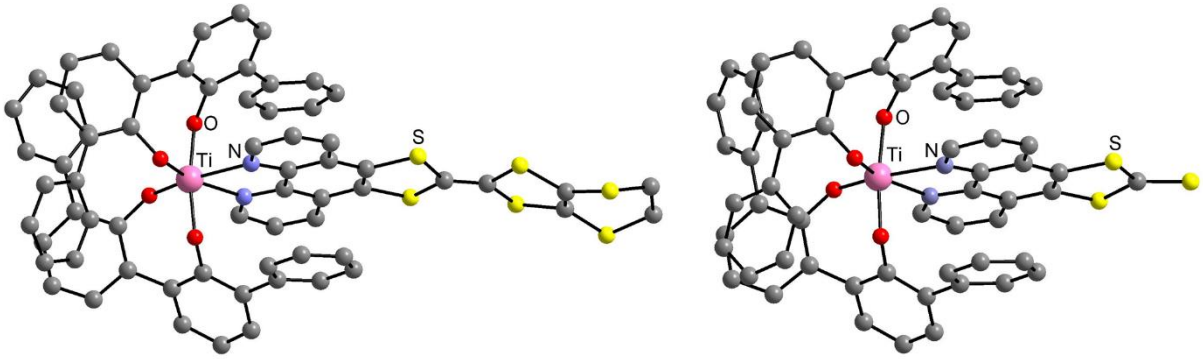

Figure 2. Ball and stick model of Ti(**1**)$_2$(**2a**) (left) and Ti(**1**)$_2$(**2b**) (right) obtained by X-ray diffraction. Hydrogen atoms and solvent molecules as well as the positional disorder of one carbon atom of the ethylenedithio bridge in Ti(**1**)$_2$(**2a**) have been omitted for clarity.

UV-visible absorption, DFT calculations

Having in hands complexes Ti(**1**)$_2$(**2a**) and Ti(**1**)$_2$(**2b**), the UV-visible light absorption properties of these species were investigated. The absorption spectra of compounds Ti(**1**)$_2$(**2a**), Ti(**1**)$_2$(**2b**), **2a** and **2b** were recorded in dichloromethane (Figure 3). Moderately intense absorption bands for Ti(**1**)$_2$(**2b**) ($\varepsilon_{max(370\ nm)}$ = 12830 L.mol^{-1}.cm^{-1}) and **2b** ($\varepsilon_{max(390\ nm)}$ = 12750 L.mol^{-1}.cm^{-1}) were measured in the range of 350-400 nm and no absorption band is noticed for the two other compounds in this region. The absorption band for Ti(**1**)$_2$(**2b**) was blue shifted of 20 nm compared to **2b**. Moreover, broad absorption bands between 420 and 520 nm concerned the absorption properties in the visible domain of Ti(**1**)$_2$(**2b**) ($\varepsilon_{max(440\ nm)}$ = 2200 L.mol^{-1}.cm^{-1}), Ti(**1**)$_2$(**2a**) ($\varepsilon_{max(440\ nm)}$ = 2700 L.mol^{-1}.cm^{-1}) and **2a** ($\varepsilon_{max(440\ nm)}$ = 1700 L.mol^{-1}.cm^{-1}). These data matched with the red-orange color of the complexes and of the ligand **2a**. Thus, such a color for the complexes was assigned to a combination of two phenomena; a ligand-to-metal charge transfer between the electrons localized on the oxygen atoms of ligand **1** and the metallic center (*vide infra*), as it is usually the case for Ti(IV) aryloxide complexes[22] and the absorption properties of ligand **2a**.

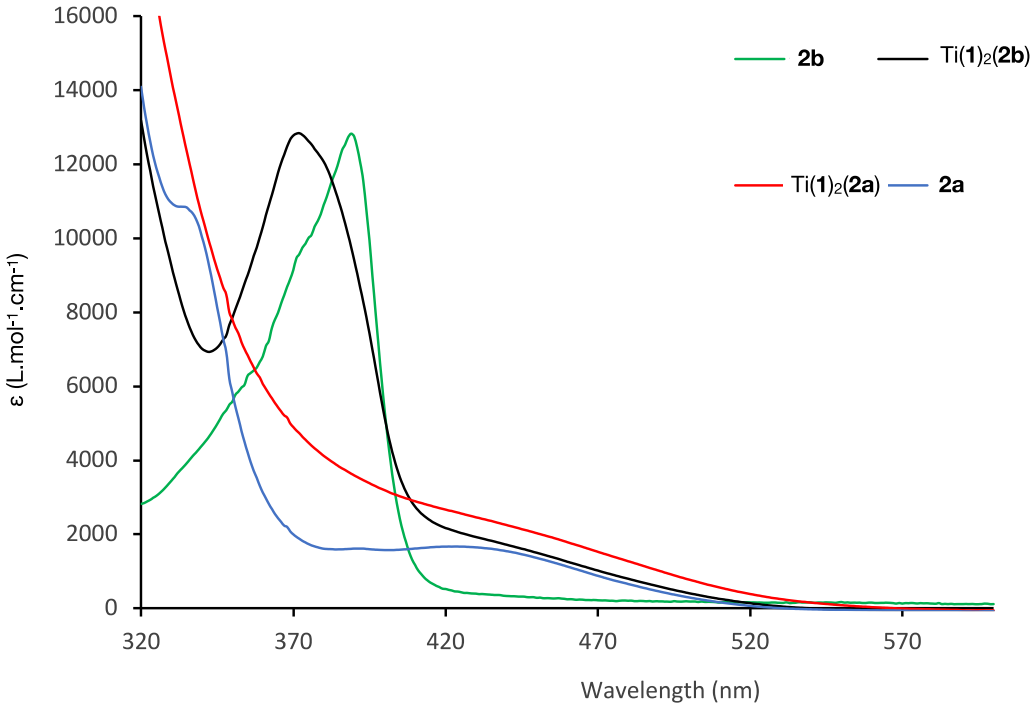

Figure 3. UV-vis spectra of **2a-b** and Ti(**1**)$_2$(**2a-b**) complexes in dichloromethane at room temperature (10^{-4} mol.L^{-1}).

To further interpret the electronic transitions in these metal complexes, we performed TD-DFT calculation applying the Tamm-Dancoff (TDA) approach, using the B3LYP hybrid functional with the Grimme D3 dispersion correction[23] and a def2-TZVP basis set[24] using the optimized geometry previously obtained of Ti(**1**)$_2$(**2a**) and Ti(**1**)$_2$(**2b**) in CH_2Cl_2, where CH_2Cl_2 was described implicitly using the PCM Model.[25] For both complexes the first 50 transitions were calculated. All calculations were performed using the GAUSSIAN09 Revision D01 software package.[26] Characteristics of all 50 calculated transitions are given in SI (Table S1 and S2) Thus, it appears that the most intense absorption band is calculated at λ = 352 nm for Ti(**1**)$_2$(**2a**), corresponding to a transition from the HOMO to the LUMO +6 level (Figure 4). The transition between these frontier orbitals is a charge transfer between electrons localized in HOMO, centered on the TTF ligand, and a LUMO level involving together the metal and the phenanthroline backbone but also with the phenyl rings of ligand **1** which are π-stacked to the phenanthroline unit. On the other hand, for the model complex Ti(**1**)$_2$(**2b**), an intense band at 337 nm is calculated that corresponds to a transition from HOMO -6 to either LUMO or LUMO +2 levels. These electronic transitions are charge transfers between the HOMO centered exclusively on the phenanthroline derivative and

the orbitals of the metallic center associated with the phenanthroline derivative (LUMO and LUMO +2) (Figure 4).[27] This investigation highlights that the introduction of the tetrathiafulvalene unit deeply affects the nature of the charge transfer associated with the most intense transitions.

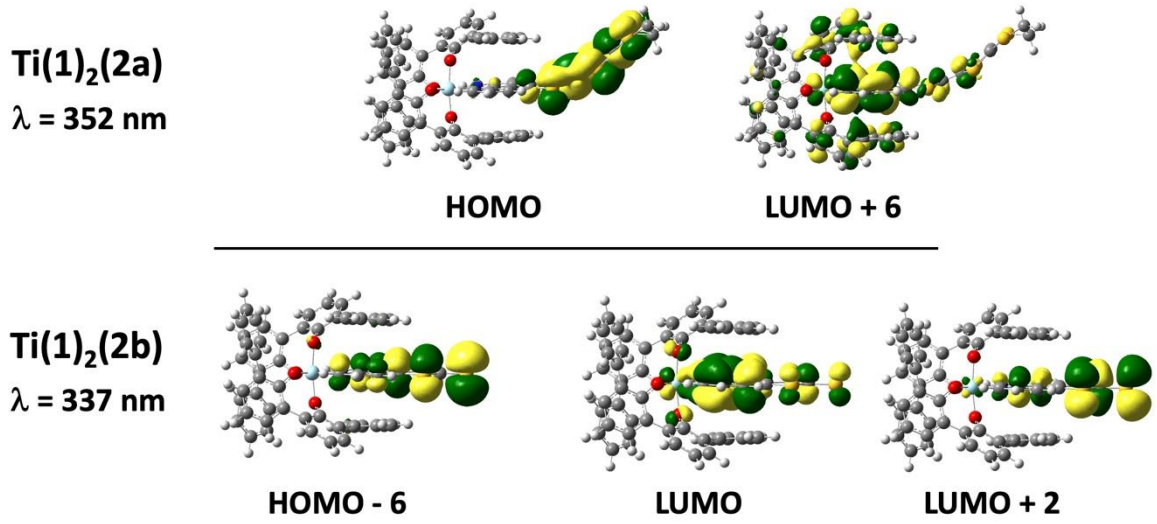

Figure 4. Representation of calculated frontier orbitals for Ti(**1**)$_2$(**2a-b**). Top row: Frontier orbitals of Ti(**1**)$_2$(**2a**) involved in the most intense absorption at λ = 352 nm. Bottom row: Frontier orbitals of Ti(**1**)$_2$(**2b**) involved in the two most intense absorptions at λ = 337 nm (more frontier orbitals for Ti(**1**)$_2$(**2a**) and Ti(**1**)$_2$(**2b**) are given in SI (Figures S8-9)).

Electrochemical and spectroelectrochemical studies

The electrochemical properties of ligand **2a** and Ti(**1**)$_2$(**2a**) in 1,2-dichloroethane solution with 0.1 mol/L NBu_4PF_6 as supporting electrolyte were investigated by cyclic voltammetry (Figure 5). **2a** exhibits two reversible one-electron redox couples which are associated with the successive oxidation of the TTF unit to $TTF^{+\bullet}$ at 0.158 V and to TTF^{2+} at 0.562 V *versus* the redox potential of Fc/Fc^+ used as an internal reference, respectively (the redox potentials are indicated in Table 2, see also the Supporting Information Figures S10-12). It should be noted that, on the reverse sweep, a narrow peak at around +0.5 V is observed and attributed to the cathodic redissolution of the strongly adsorbed oxidized products of the TTF. The irreversible reduction at -1.971 V for **2a** corresponds to the reduction of the phenanthroline unit (Phen) leading to the radical anion ($Phen^{-\bullet}$).

Ti(**1**)$_2$(**2a**) exhibits a similar behavior in the anodic domain. The electrochemical patterns of Ti(**1**)$_2$(**2a**) consist of two oxidative processes at 0.269 V and at 0.626 V *versus* Fc/Fc$^+$ (Figure 5). The first oxidation is again assigned to the monoelectronic TTF unit oxidation forming the radical monocation TTF$^{+\bullet}$, while the second oxidation wave is attributed to the oxidation of the radical monocation TTF$^{+\bullet}$ leading to the dication TTF^{2+} formation. Accordingly, upon coordination to the titanium(IV), the first two reversible oxidation processes are slightly shifted to a positive value in comparison with the free ligand. On the cathodic scan, one reduction wave at −1.724 V is detected. This reduction is assigned to the Ti(IV) to Ti(III) one electron-reduction process since, for the model complex Ti(**1**)$_2$(**2b**), a reduction wave associated to the Ti(IV) to Ti(III) at a very similar potential was measured (Table 1) (*vide infra*). X-band EPR experiments have been performed on Ti(**1**)$_2$(**2a**) to confirm the assignation. Initially the solution is EPR silent. After one-electron oxidation at 0.27 V, the spectrum shows a narrow signal, centered at g-value of 2.00, typical of an organic radical (Figure S16). After exhaustive reduction performed at around −1.73 V, the spectrum exhibits an anisotropic signal with rhombic g-values of g_x = 1.99, g_y = 1.93 and g_z = 1.82 (Figure 6). These values are typical of Ti(III) ion in distorted octahedral geometry.[28] It asserts that the first oxidation is centered on the ligand, whereas the reduction of the complex leads to the formation of a Ti(III) center.

Table 1. Electrochemical data for proligand **1**H$_2$ (2,2'-biphenol derivative), phenanthroline **2a-b** and complexes Ti(**1**)$_2$(**2a-b**) *versus* Fc/Fc$^+$, and are uncorrected for ohmic drop.

Compounds	Oxidation		Ti(IV)/Ti(III) couple	Phenanthroline reduction
1H$_2$		1.368^{irr}	-	-
2a	0.562 (108)	0.158 (93)		-1.971^{irr}
2b		0.927^{irr}		-1.991^{irr}
Ti(**1**)$_2$(**2a**)	0.626 (97)	0.269 (72)	-1.724 (122)	-2.031 (138)
Ti(**1**)$_2$(**2b**)		0.706^{irr}	-1.705 (89)	-2.035 (141)

Potentials in V *vs.* Fc/Fc$^+$ were obtained from cyclic voltammetry in 1,2-$C_2H_4Cl_2$ with 0.1

mol.L^{-1} NBu_4PF_6. Scan rate = 100 mV s^{-1}. Working electrode: GC, d= 3 mm. The given half-wave potentials are equal to $E_{1/2} = (E_{pa} + E_{pc})/2$. Under bracket: $\triangle E_p = |E_{pa}-E_{pc}|$.

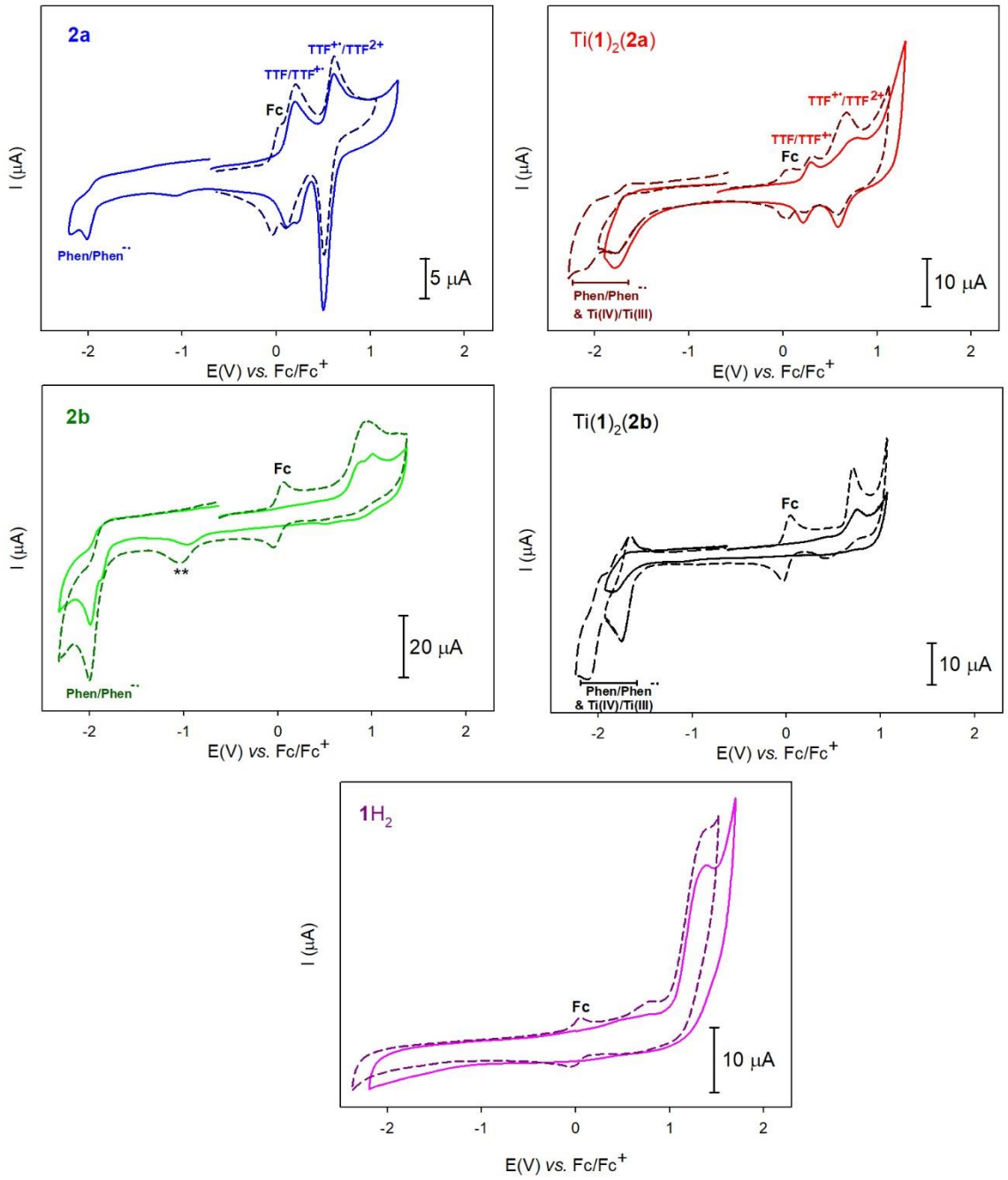

Figure 5. Cyclic voltammetry of proligand **1**H_2 (2,2'-biphenol derivative), phenanthroline **2a-b** and complexes Ti(**1**)$_2$(**2a-b**) in 0.1 mol.L^{-1} n-Bu_4NPF_6/1,2-$C_2H_4Cl_2$ at scan rates of 0.1 V.s^{-1} on glassy carbon GC electrode in the absence (full line) and presence (dashed line) of Fc in solution. The Fc^+/Fc redox potential is used as internal standard reference of the potential axis.

In addition to cyclic voltammetry, solution spectroelectrochemical studies were carried out to investigate the electronic properties of all the electrochemically generated species (Figures 7–8). The UV-Vis-NIR spectro-electrochemical studies of ligand **2a** and Ti(**1**)$_2$(**2a**) have been performed over reduction-oxidation cycles (Figure 7).

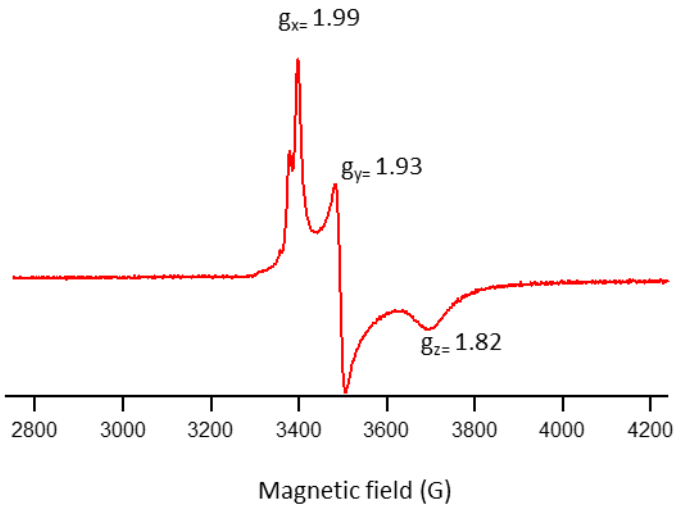

Figure 6. X-band EPR spectrum of a solution of Ti(**1**)$_2$(**2a**) in 0.1 mol.L^{-1} n-Bu_4NPF_6/1,2-$C_2H_4Cl_2$ recorded at 100K after exhaustive electrolysis performed at the first reduction peak.

In the case of ligand **2a** and Ti(**1**)$_2$(**2a**) (Figure 7), the electrochemical oxidation of the TTF unit induces strong changes in the UV–vis–NIR absorption spectra. For **2a**, in the neutral state, five absorbance bands are detected at 233, 277, 311, 335 and 423 nm (weak). The energy transitions are in good agreement with those reported for TTF compounds. Bands at 311 and 335 nm represent the transitions from the HOMO (π) to the LUMO (σ*) and from the HOMO to LUMO+1 π → π * respectively.[29] For **2a**, upon oxidation to the cation radical state $TTF^{+\bullet}$ unit, a decrease in the absorbance bands at 277, 311 and 335 nm is observed with the appearance and concomitant increase of new absorbance bands at 452, 476, 547, and 909 nm (red curve of Figure 7). An isosbestic point is found at 372 nm (Figure 7) indicating that conversion from TTF to $TTF^{+\bullet}$ is a direct reaction with no side products or intermediates. It should be noted that the band found at low energy is in accordance with the absorption properties reported for a cationic radical TTF dimer $(TTF^{+\bullet})_2$.[30] Thus, the absorption spectrum of the oxidized **2a** ligand was interpreted as the result of the simultaneous presence of **2a**$^{+\bullet}$ and (**2a**$^{+\bullet}$)$_2$. It can be noted that the cyclic voltammograms, measured using an Au grid working

electrode during the spectroelectrochemical measurements, indicate that the first oxidation is reversible. The resulting absorption spectrum from reduction of the cation radical $TTF^{+\bullet}$ back to the neutral TTF unit supports this assumption with almost complete reversibility detected on the time scale of the spectroelectrochemical experiment (around 150 s in the case of Figure 7).

Upon gradual oxidation to the dicationic species TTF^{2+}, no change of the optical spectra has been observed. It may be due to the strong adsorption of the oxidized species with TTF^{2+} on the electrode, as already observed during the cyclic voltammetry measurements.

Upon investigation by UV−vis−NIR spectroelectrochemical experiments, complex Ti(**1**)$_2$(**2a**). Ti(**1**)$_2$(**2a**) exhibited a behavior similar to **2a**. Upon oxidation to the cation radical state of the TTF unit, the decrease of the three bands at 262, 315 and 339 nm (shoulder) occurs concomitantly to the increase of the four bands at 441, 475, 559 and 915 nm. When the potential reaches the second oxidation of the TTF unit, again no change of the optical spectrum was observed. This can be again attributed to the strong adsorption of the oxidation product on the Au minigrid electrode as already mentioned for **2a**.

With the Au minigrid working electrode, one quasi-reversible wave is detected at -1.517 V *versus* Ag/AgCl during the cathodic scan. This wave corresponds to the reversible wave measured at -1.724 V *versus* Fc/Fc^+ by cyclic voltammetry on glassy carbon electrode. Upon reduction at -1.517 V *versus* Ag/AgCl the decrease of the band at 263 nm is associated to the emergence of five bands at 229, 339, 430, 561 and 1412 nm (weak). It can be attributed to the reduction of the Ti(IV) to Ti(III).

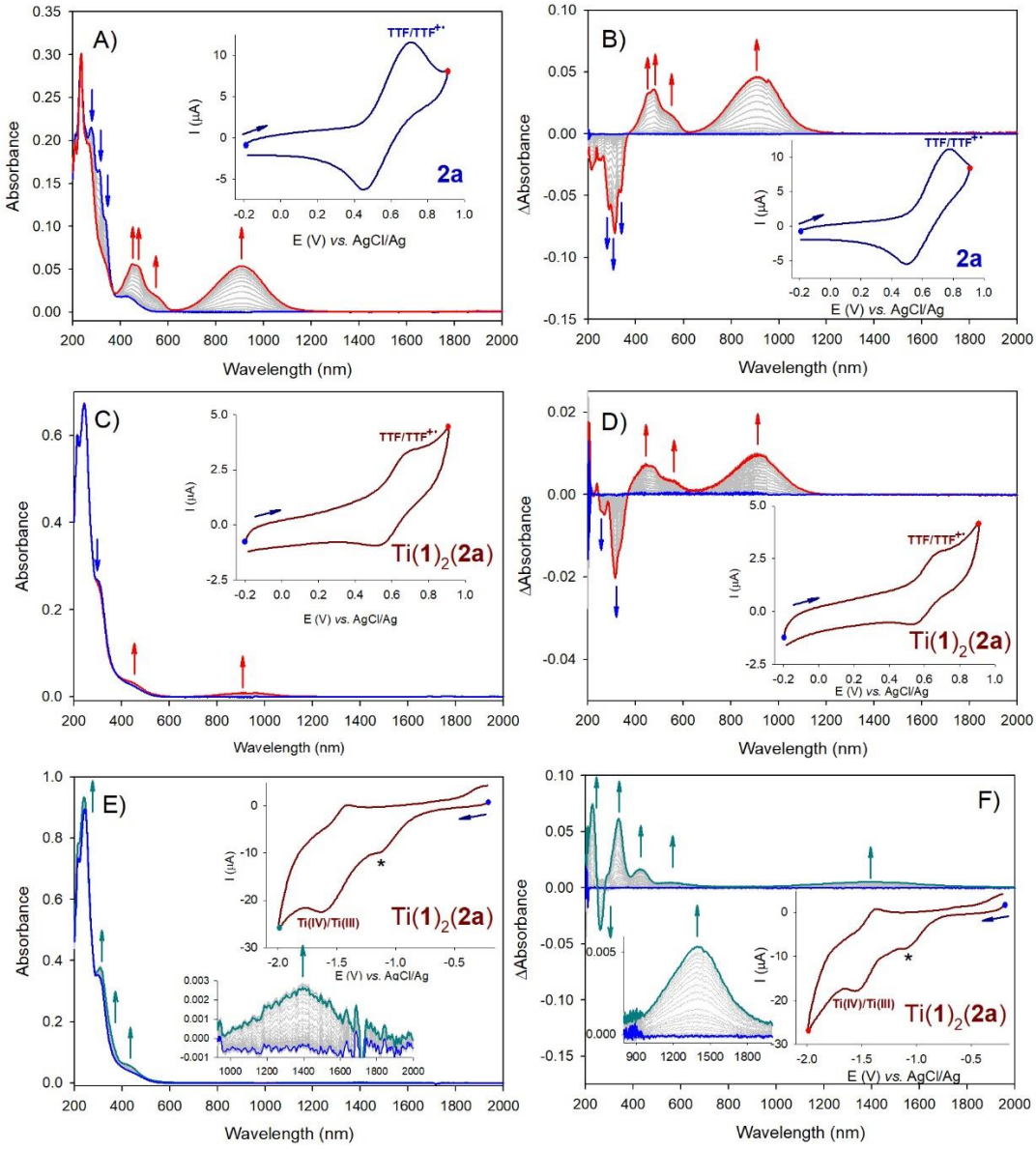

Figure 7. A) UV-Vis spectroelectrochemistry and B) the differential UV-Vis-NIR spectra of **2a** at ambient temperature upon electrochemical oxidation in 0.1 mol.L^{-1} n-Bu_4NPF_6 in 1,2-$C_2H_4Cl_2$ in the potential region of the first oxidation step (one-electron oxidation leading to the radical cation TTF Blue color corresponds to the spectra of initial compound while red color is for the oxidized form. C) UV-Vis spectroelectrochemistry and D) the corresponding differential UV-Vis-NIR spectra of Ti(**1**)$_2$(**2a**) upon the first oxidation step. E) UV-Vis spectroelectrochemistry and F) the differential UV-Vis-NIR spectra of Ti(**1**)$_2$(**2a**) upon electrochemical reduction in 0.1 mol.L^{-1} n-Bu_4NPF_6 in 1,2-$C_2H_4Cl_2$ (reduction of the phenanthroline moieties leading to the radical anion). Blue color corresponds to the spectra of initial **2a** while dark cyan color is for the reduced form. Inset figures shows the cyclic voltammograms at scan rate of 20 mV.s^{-1} and

the potentials (colored circles) at which the UV-Vis-NIR spectra were taken. * Corresponds to the residual O_2 reduction on the Au minigrid working electrode.

The electrochemical properties of ligand **2b** and the model complex Ti(**1**)$_2$(**2b**) have been also investigated by cyclic voltammetry in 1,2-dichloroethane solution with 0.1 mol.L^{-1} NBu_4PF_6 as supporting electrolyte (Figure 5). Ligand **2b** shows one oxidation and one reduction irreversible processes at 0.927 and -1.991 V respectively. The reduction at -1.991 V is attributed to the reduction of the phenanthroline ligand (Phen) forming the radical anion (Phen$^{\bullet -}$), while the oxidation wave corresponds probably to the irreversible oxidation of the C=S double bond. Concerning the model complex Ti(**1**)$_2$(**2b**), the reduction of titanium(IV) to titanium (III) is measured at nearly the same potential (-1.705 V *vs.* Fc/Fc$^+$) as for Ti(**1**)$_2$(**2a**) (-1.724 V *vs.* Fc/Fc$^+$). The second reduction wave measured at -2.035 V (see in the Supporting Information Fig. S12 and Table 2) is ascribed to the reduction of the phenanthroline unit (Phen) leading to the formation of the radical anion Phen$^{\bullet -}$. Consequently, the presence of the TTF core in the complex did not influence the reduction potential of the metallic center.
UV−vis−NIR spectroelectrochemical experiments were also performed with Ti(**1**)$_2$(**2b**) (Figure 8). Upon reduction at -1.713 V *versus* Ag/AgCl using Au minigrid working electrode (corresponding to the wave measured at -1.705 V *versus* Fc/Fc$^+$ with GC electrode), the reduction of Ti(IV) to Ti(III) is associated to the decrease of the intensity of the bands at 259, 309 and 374 nm concomitantly with the emergence of six bands at 228, 285, 334, 410 and 1384 nm caused by the reduction of Ti(IV) to Ti(III).

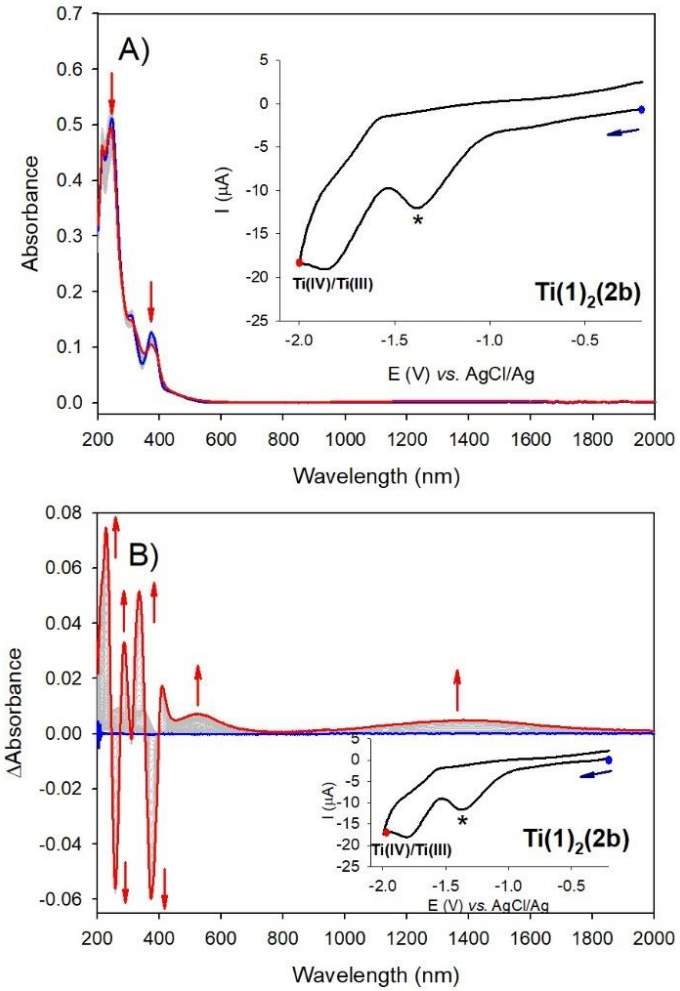

Figure 8. A) UV-Vis-NIR spectroelectrochemistry and B) the corresponding differential UV-Vis-NIR spectra of the model complex Ti(**1**)$_2$(**2b**) at ambient temperature upon electrochemical reduction in 0.1 mol.L^{-1} n-Bu_4NPF_6 in 1,2-$C_2H_4Cl_2$ in the potential region of the first and second oxidation step at scan rate of 20 mV.s^{-1} . Insert figures show the CV at scan rate of 20 mV.s^{-1}. Blue color corresponds to the spectra of initial compounds Ti(**1**)$_2$(**2b**) while red color is for the oxidized form. * Corresponds to the residual O_2 reduction onto the Au minigrid working electrode.

Photophysical studies

The photophysical properties of complexes Ti(**1**)$_2$(**2a**-**c**) were investigated in deoxygenated CH_2Cl_2. Prior to these analyses, the emission properties of the phenanthroline based ligands were investigated in the same solvent. Upon excitation at 310 nm, 1,10-phenanthroline exhibits a structured fluorescence spectrum with a maximum at 350 nm, and an emission

decay of 2.3 ns ± 0.1 ns. This emission is attributed to a mixed (n,π*);(π,π*) state and is consistent with previously reported values recorded in different solvents.[31] In the same experimental conditions, compound **2a** is non-emissive. This indicates an efficient interaction between the excited state of phenanthroline and the TTF subunit. TTF is known as a high π donor compound and the interaction results from an electron transfer process from TTF to the excited state of phenanthroline, leading to a non-emissive (Phen$^{\bullet-}$-TTF$^{\bullet+}$) charge transfer state.

Complexes Ti(**1**)$_2$(**2a**-**c**) are all emissive upon excitation at 310 nm. The emission is broad and centered around 360 nm. In comparison to references complexes Ti(**1**)$_2$(**2b**) and Ti(**1**)$_2$(**2c**), the emission maximum of Ti(**1**)$_2$(**2a**) is red shifted (see Figures S13-15 in SI and Table 2). Upon excitation in the visible at 405 nm, the complexes exhibit a weak emission band centered at 440 nm for complexes Ti(**1**)$_2$(**2b**) and Ti(**1**)$_2$(**2c**) and at 480 nm for complex Ti(**1**)$_2$(**2a**). After excitation at 405 nm the emission decays are biexponential. The biexponential rate indicates that two states are contributing to the observed emission. The short component of the decay around 2 ns represents between 34 % and 62 % of the overall intensity. The longer component varies with the complex and is significantly longer for Ti(**1**)$_2$(**2a**) (Table 2). Since the short component has an almost similar lifetime within the series of complexes, it could be attributed to the deactivation of the (Ti(**1**)$_2$)* moiety upon excitation. The longer component of the decay would then correspond to the deactivation of an excited state involving the phenanthroline based ligand. Whereas excitation of ligand **2a** leads to a none emissive (Phen$^{\bullet-}$-TTF$^{\bullet+}$) state, excitation of Ti(**1**)$_2$(**2a**) at 405 nm induces the population of an emissive state localized on the Ti(**2a**) moiety. The difference in the photophysical behavior between the free ligand and the complex suggests then a partial contribution of the molecular orbitals of the Ti center on the emissive excited state. Moreover, compared to Ti(**1**)$_2$(**2b**) and Ti(**1**)$_2$(**2c**), the emission decay in Ti(**1**)$_2$(**2a**) is slightly longer as a probable consequence of an electron transfer process following eq. 3 and leading to a charge separated state on a longer distance as supported by EPR measurements (Figure 6). The recombination of the charge occurs then on a longer time scale of 12.7 ns compared to around 7 ns for the reference complexes.

$$[(\mathbf{1})_2\text{Ti(IV)(phen-TTF)}] \xrightarrow{405\ nm} [((\mathbf{1})_2\text{Ti(III)phen-TTF}^{\bullet+})] \quad \text{(eq. 3)}$$

Table 2. Photophysical data for complexes Ti(**1**)$_2$(**2a-c**) recorded in deoxygenated CH_2Cl_2.

Compounds	$\lambda_{max.}$ em.		Emission lifetime
	Exc. 310 nm	Exc. 405 nm	Exc. 405 nm
Ti(**1**)$_2$(**2a**)	370	480	2.1 ns ± 0.2 (34%) ; 12.7 ns ± 0.4 (66%)
Ti(**1**)$_2$(**2b**)	354	436	1.5 ns ± 0.1 (63%) ; 7.4 ns ± 0.3 (37%)
Ti(**1**)$_2$(**2c**)	356	440	1.8 ns ± 0.1 (48%) ; 6.9 ns ± 0.3 (52%)

Conclusion

To get a deep understanding of the interaction between a TTF unit and a Ti(IV) center, the monomeric heteroleptic Ti(**1**)$_2$(**2a**) complex was prepared. The introduction of a TTF unit modifies the electronic properties related to the model complex Ti(**1**)$_2$(**2b**) as demonstrated by the UV-visible absorption measurements. In the case of Ti(**1**)$_2$(**2a**), the most intense transitions are originated from HOMOs centered on the TTF unit and LUMOs involving mostly the d orbitals of the metal and the phenanthroline fragment, while for the model complex Ti(**1**)$_2$(**2b**), the most intense transition results from charge transfers between the HOMO localized on the phenanthroline fragment and the orbitals centered on both the metallic center and the phenanthroline derivative. Concerning the electrochemical properties of ligand **2a**, its coordination to the metallic center only weakly modifies its oxidation potentials and a similar oxidation pattern consisting of two quasi-reversible oxidative processes is observed for the free ligand and Ti(**1**)$_2$(**2a**). The reduction waves of Ti(IV) to Ti(III) were found to be similar for Ti(**1**)$_2$(**2b**) and Ti(**1**)$_2$(**2a**) and the EPR measurement for Ti(**1**)$_2$(**2a**) clearly confirmed that the first reduction process induced the formation of a Ti(III) species and permitted to exclude the reduction of a ligand within Ti(**1**)$_2$(**2a**). Furthermore, the presence of the TTF core in Ti(**1**)$_2$(**2a**) does not affect the reduction potential of the metal atom. Hence, from the electrochemical properties, the TTF unit as well as the Ti(IV) center could be considered as almost two independent chemical entities within the same architecture. The photophysical studies supported by the conclusions obtained from the electrochemistry and EPR measurements

suggest the occurrence of an electron transfer process upon visible light excitation in Ti(**1**)$_2$(**2a**) between the donor part of the molecule (TTF) and the acceptor (the metal d orbitals combined with a contribution of the phenanthroline fragment) forming the charge separated state [((**1**)$_2$Ti(III)phen-TTF$^{\bullet+}$)] that recombines afterward. Overall, the TTF unit and the Ti(IV) center look as an appealing combination to create new dyads. Thus, we envisage now to introduce various chemical spacers between the TTF unit and the diimine ligand to modulate the electronic transfer/recombination events in our TTF-Ti(IV) system. Current efforts are focusing on this task.

Supporting Information: ^{1}H NMR and ^{13}C spectra for the two complexes, crystal packing for the structures of Ti(**1**)$_2$(**2a**) and Ti(**1**)$_2$(**2b**), representation of the frontier orbitals calculated for Ti(**1**)$_2$(**2a**) and Ti(**1**)$_2$(**2b**), voltammograms and EPR spectrum of the oxidized Ti(**1**)$_2$(**2a**) complex.

Experimental part

All reagents and products were purchased from Sigma-Aldrich, Alfa Aesar, or TCI and used as received. Bruker Avance-500 and Avance-600 spectrometers were used for solution NMR analyses performed at 25 °C. Deuterated solvents for ^{1}H NMR analysis were dried over molecular sieves before use. ^{1}H NMR spectra were recorded at 500.13 MHz and referenced to $SiMe_4$. $^{13}C\{^1H\}$ NMR spectra (broadband decoupled) were recorded at 126.77 MHz and referenced to $SiMe_4$. Chemical shifts are reported in parts per million and coupling constants in hertz; the latter are proton−proton coupling constants. Multiplicity: s = singlet, d = doublet, t = apparent triplet, and m = multiplet. The $^{13}C\{^1H\}$ signals are singlets. DOSY measurements were performed at 600.13 MHz with a 5 mm ^{1}H/X *z*-gradient BBI probe and applying a PFGSTE pulse sequence using bipolar gradients. Electrospray analyses were performed on a MicroTOF (Bruker) apparatus equipped with an electrospray source. Elemental analyses were performed using a Flash 2000 apparatus (Thermo Fisher Scientific) for the C, H, and N elements. UV−visible liquid spectra were recorded with a PerkinElmer Lambda 650s spectrometer. For Ti(**1**)$_2$(**2a**), X-ray diffraction data collection was carried out at 120 K on a Bruker PHOTON III DUO CPAD diffractometer equipped with an Oxford Cryosystem liquid N_2 device, using Mo-Kα radiation (λ = 0.71073 Å). The X-ray diffraction data for Ti(**1**)$_2$(**2b**) were collected at 173 K on a

Bruker SMART CCD diffractometer with Mo Kα radiation (λ = 0.71073 Å). The diffraction data were corrected for absorption using the *SADABS* program.[30] The structures were solved using SHELXS97 and refined by full-matrix least squares on F^2 using SHELXL-2014.[31] The H atoms were introduced at calculated positions and not refined (riding model). Compound **2a** and complex Ti(**1**)$_2$(HO^{i}Pr)$_2$ were prepared as described.[19,20]

Electrochemical and spectroelectrochemical measurements

Electrochemistry

Electrochemistry Materials: Pure 1,2-$C_2H_4Cl_2$ from Sigma-Aldrich (anhydrous, purity >99.8%) was used throughout. 0.1 mol.L^{-1} N(Bu)$_4$PF$_6$ from Sigma-Aldrich was used as a supporting electrolyte.

Electrochemistry measurements: Electrochemical measurements were carried out in 1,2-$C_2H_4Cl_2$ containing 0.1 mol.L^{-1} N(Bu)$_4$PF$_6$ in a classical three-electrode cell by cyclic voltammetry and rotating-disk voltammetry.

Cyclic voltammograms (CV) were recorded in a standard three-electrode electrochemical cell using glassy carbon disk (GC) (3 mm in diameter) as working electrode, Pt wire as counter electrode, and AgCl or Pt wire as reference or pseudo-reference electrode. The cell was connected to an Autolab PGSTAT30 potentiostat (Eco Chemie, Netherlands) driven by a GPES software running on a personal computer. All potentials are given *versus* AgCl/Ag, which were used as internal references, and are uncorrected for ohmic drop.

UV-Vis-NIR spectroelectrochemistry

In situ UV-Vis-NIR spectroelectrochemical measurements at room temperature were performed with an optically transparent thin-layer electrochemical (OTTLE) cell equipped with an Au minigrid working electrode and CaF_2 optical windows.[32] UV-Vis-NIR spectroelectrochemical analyses have been carried out with a Zeiss MCS 601 UV-Vis-NIR diode array spectrometer. Spectrophotometric analyses of the films have been conducted using a 0.1 mol.L^{-1} solution of n-Bu$_4$NPF$_6$ in anhydrous 1,2-$C_2H_4Cl_2$ in deoxygenated solutions. The reference used is AgCl/Ag.

EPR

The experiments are performed with an EMX Plus spectrometer and a Bruker ER4119HS cavity at a microwave power of 0.007 mW.

Photophysics

Emission Spectra were recorded with a Fluoromax-4 (Horiba Scientific) in a 1 cm quartz cuvette. Samples were purged with Ar for 15 minutes prior to experiment and closed with a septum. Emission decay were recorded with a PicoHarp 300 time-correlated single photon counting (TCSPC) system. The samples were excited at 405 nm by a laser diode. The fittings of the decays were performed with FluoFit software (PicoQuant).

General Procedure for the synthesis of Ti(1)$_2$(2a) and Ti(1)$_2$(2b).

Complexes **Ti(1)$_2$(2a)** and **Ti(1)$_2$(2b)** have been synthesized following two different methods using a titanium complex precursor Ti(**1**)$_2$(HO^{i}Pr)$_2$. **Method a** or a one pot strategy **Method b** leading to similar yields.

Synthesis of Ti(1)$_2$(2a)

Method a: To a solution of dried CH_2Cl_2 (4 mL) and Ti(**1**)$_2$(HO^{i}Pr)$_2$ (5 mg, 5.95 mmol) under inert atmosphere (glovebag filled with Ar), phenanthroline derivative **2a** (2.7 mg, 5.95 mmol) was added. The resulting red mixture was purified by silica gel column chromatography with CH_2Cl_2/*n*-pentane (2:3) as eluent to afford the desired red solid **Ti(1)$_2$(2a)** (64%, 4.5 mg).

Method b: To a solution of dried CH_2Cl_2 (2 mL), Ti(O^{i}Pr)$_4$ (7.2 µL, 24.5 mmol) under inert atmosphere (glovebag filled with Ar), **1**H_2 (15 mg, 49.0 mmol) and phenanthroline derivative **2a** (11 mg, 24.5 mmol) were added at the same time. The colorless solution became instantly red, and the resulting mixture was purified by silica gel column chromatography with CH_2Cl_2/*n*-

^{1}H NMR (500 MHz, $CDCl_3$) δ 8.54 (dd, *J* = 5.0, 1.4 Hz, 2H), 7.57 (dd, *J* = 8.3, 1.5 Hz, 2H), 7.41 (dd, *J* = 7.2, 1.3 Hz, 4H), 7.23 (dt, *J* = 7.6, 1.3 Hz, 2H), 7.20 (d, *J* = 4.4 Hz, 2H), 7.11 – 7.06 (m, 4H), 6.98 (dddd, *J* = 7.5, 6.1, 3.3, 1.0 Hz, 6H), 6.94 – 6.90 (m, 2H), 6.50 (t, *J* = 7.6 Hz, 2H), 6.41 (dd, *J* = 7.5, 1.8 Hz, 2H), 6.32 (d, *J* = 7.4 Hz, 6H), 6.26 (dd, *J* = 8.2, 6.6 Hz, 4H), 3.21 (d, *J* = 1.4 Hz, 4H). ^{13}C NMR (126 MHz, $CDCl_3$) δ 160.89, 160.18, 148.95, 141.28, 138.88, 138.72, 134.73, 132.00, 131.57, 131.42, 130.02, 129.92, 129.76, 129.72, 128.84, 128.67, 127.90, 127.86, 127.55, 126.09, 125.93, 124.60, 123.96, 122.04, 119.29, 30.31.

HRMS (ESI-MS): m/z Calcd for $C_{66}H_{42}N_2O_4S_6Ti$, 1167.0951 $[M]^+$; Calcd for $C_{66}H_{43}N_2O_4S_6Ti$, 1167.1029 $[M+H]^+$; found, 1167.1013.

Crystal data for $C_{80}H_{58}N_2O_4S_6Ti$, monoclinic, $P2_1/n$, a = 15.8580(5) Å, b = 23.7325(7) Å, c = 17.1275(6) Å; β = 92.9140(10°), V = 6437.6(4) Å^3; Z = 4; D_{calcd} = 1.394 g.cm^{-3}; T = 120(2) K, μ = 0.384 mm^{-1}, reflections collected 130396, unique reflections 15435 (R_{int} = 0.0973), R_1(F) [I > 2σ(I)] = 0.0537, wR$_2$(F²) (all data) = 0.1515; GOF(F²) = 1.010.

Synthesis of Ti(1)$_2$(2b)

The same procedure has been followed using **2b** instead of **2a** to synthesize the orange complex **Ti(1)$_2$(2b)** with a yield of 50% for **Method a & b**. Suitable crystals for X-ray diffraction were obtained from CH_2Cl_2/*n*-pentane gas diffusion.

^{1}H NMR (500 MHz, $CDCl_3$) δ 8.73 (dd, J = 5.0, 1.4 Hz, 2H), 7.74 (dd, *J* = 8.2, 1.4 Hz, 2H), 7.50 – 7.46 (m, 4H), 7.32 (dd, *J* = 7.7, 1.8 Hz, 2H), 7.28 (dd, *J* = 7.7, 1.8 Hz, 2H), 7.23 (dd, *J* = 8.5, 5.0 Hz, 2H), 7.18 (dd, *J* = 7.6, 1.8 Hz, 2H), 7.12 – 7.03 (m, 6H), 7.03 – 6.97 (m, 2H), 6.60 (t, *J* = 7.5 Hz, 2H), 6.51 (dd, *J* = 7.6, 1.8 Hz, 2H), 6.46 – 6.42 (m, 4H), 6.42 – 6.37 (m, 2H), 6.31 (m, 4H). ^{13}C NMR (126 MHz, $CDCl_3$) δ 205.82, 160.85, 160.08, 150.03, 141.45, 138.94, 138.79, 136.29, 134.59, 132.23, 131.44, 130.08, 129.88, 129.84, 129.61, 128.83, 128.73, 127.96, 127.59, 126.07, 126.00, 124.77, 124.43, 122.68, 122.25, 119.48.

HRMS (ESI-MS): m/z Calcd for $C_{61}H_{39}N_2O_4S_3Ti$, 1007.1551 $[M+H]^+$; found, 1007.1554.

Anal. Calc. for $C_{61}H_{38}N_2O_4S_3Ti$ + ½ $CHCl_3$, N, 2.63%; C, 69.25%; H, 3.64%; Found N, 2.55%; C, 69.22%; H, 3.78%.

Crystal data for $C_{63}H_{42}Cl_4N_2O_4S_3Ti$, monoclinic, $P2_1/c$, a = 28.4495(15) Å, b = 14.3729(7) Å, c = 29.2006(16) Å; β = 115.356(2)°, V = 10789.9 Å^3; Z = 8; D_{calcd} = 1.449 g.cm^{-3}; T = 173(2) K, μ = 0.526 mm^{-1}, reflections collected 115904, unique reflections 31625 (R_{int} = 0.0812), R_1(F) [I > 2σ(I)] = 0.0561, wR$_2$(F²) (all data) = 0.1461; GOF(F²) = 1.018.

Acknowledgments

Financial support from the University of Strasbourg, CNRS and the Ministère de l'Enseignement Supérieur et de la Recherche is gratefully acknowledged. We thank Nathalie Gruber (University of Strasbourg, France) for the crystal structure determination of complex **Ti(1)$_2$(2a)** and Florian Molton (DCM, University of Grenoble Alpes) for the EPR experiments and analysis. We thank Christophe Gourlaouen for fruitful discussions on TD-DFT and TDA methods.

References

[1] Fujishima, A.; Honda, K. Electrochemical Photolysis of Water at a Semiconductor Electrode. *Nature* **1972**, *238*, 37-38.

[2] Ni, M.; Leung, M. K.H.; Leung, D. Y. C.; Sumathy, K. A review and recent developments in photocatalytic water-splitting using for hydrogen production. *Renewable Sustainable Energy Rev.* **2007**, *11*, 401-425.

[3] a) Linsebigler, A. L.; Lu, G.; Yates, J. T. Photocatalysis on TiO_2 Surfaces: Principles, Mechanisms, and Selected Results. *Chem. Rev.* **1995**, *95*, 735-758; b) Bai, Y.; Mora-Seró, I.; De Angelis, F.; Bisquert, J.; Wang, P. Titanium Dioxide Nanomaterials for Photovoltaic Applications. *Chem. Rev.* **2014**, *114*, 19, 10095-10130.

[4] a) Huang, J.-F.; Lei, Y.; Luo, T.; Liu, J.-M. Photocatalytic H_2 Production from Water by Metal-free Dye-sensitized TiO_2 Semiconductors: The Role and Development Process of Organic Sensitizers. *ChemSusChem* **2020**, *13*, 5863-5895; b) Le-Quang, L.; Stanbury, M.; Chardon-Noblat, S.; Mouesca, J.-M.; Maurel, V.; Chauvin, J. Immobilization of Mn(I) and Ru(II) polypyridyl complexes on TiO_2 nanoparticles for selective photoreduction of CO_2 to formic acid. *Chem. Commun*. **2019**, *55*, 13598-13601.

[5] Duvva, N.; Chilakamarthia, U.; Giribabu, L. Recent developments in tetrathiafulvalene and dithiafulvalene based metal-free organic sensitizers for dye-sensitized solar cells: a mini-review. *Sustainable Energy Fuels* **2017**, *1*, 678-688.

[6] Tiwari, A.; Duvva, N.; Navakoteswara Rao, V.; Muthukonda Venkatakrishnan, S.; Giribabu Ujjwal Pal, L. Tetrathiafulvalene Scaffold-Based Sensitizer on Hierarchical Porous TiO_2: Efficient Light-Harvesting Material for Hydrogen Production. *J. Phys. Chem. C* **2019**, *123*, 70-81.

[7] a) Hou, J.-L.; Weng, Y.-G.; Liu, P.-Y.; Cui, L.-N.; Zhu, Q.-Y.; Dai, J. Effects of the Ligand Structures on the Photoelectric Activities, a Model Study Based on Titanium–Oxo Clusters Anchored with S-Heterocyclic Ligands. *Inorg. Chem.* **2019**, *58*, 2736; b) Yin, J.-X.; Huo, P.; Wang, S.; Wu, J.; Dai, J. A tetrathiafulvalene-grafted titanium-oxo-cluster material: self-catalyzed crystal exfoliation and photocurrent response properties. *J. Mat. Chem. C* **2015**, *3*, 409-415.

[8] Camerel, F.; Jeannin, O.; Yzambart, G.; Fabre, B.; Lorcy, D.; Fourmigue, M. Redox-active proligands from the direct connection of 1,3-dithiol-2-one to tetrathiafulvalene (TTF): syntheses, characterizations and metal complexation. *New J. Chem.* **2013**, *37*, 992-1001

[9] a) Kulyk, O.; Rocard, L.; Maggini, L.; Bonifazi, D. Synthetic strategies tailoring colours in multichromophoric organic nanostructures. *Chem. Soc. Rev.* **2020**, 49, 8400-8424; b) Frischmann, P. D.; Mahata, K.; Würthner, F. Powering the future of molecular artificial photosynthesis with light-harvesting metallosupramolecular dye assemblies. *Chem. Soc. Rev.*, **2013**, *42*, 1847-1870.

[10] a) Lentz, C.; Schott, O.; Auvray, T.; Hanan, G.; Elias, B. Photocatalytic Hydrogen Production Using a Red-Absorbing Ir(III)–Co(III) Dyad. *Inorg*. *Chem.* **2017**, *56*, 18, 10875-10881; b) Reichardt, C.; Sainuddin, T.; Wächtler, M.; Monro, S.; Kupfer, S.; Guthmuller, J.; Gräfe, S.; McFarland, S.; Dietzek, B. Influence of Protonation State on the Excited State Dynamics of a Photobiologically Active Ru(II) Dyad. *J. Phys. Chem. A* **2016**, *120*, 32, 6379-6388; c) Li, T.-T.; Li, F.-M.; Zhao, W.-L.; Tian, Y.-H.; Chen, Y.; Cai, R.; Fu, W.-F. Highly Efficient and Selective Photocatalytic Oxidation of Sulfide by a Chromophore–Catalyst Dyad of Ruthenium-Based Complexes. *Inorg*. *Chem*. **2015**, *54*, 1, 183-191; d) Costa, R. D.; Céspedes-Guirao, F. J.; Bolink, H. J.; Fernández-Lázaro, F.; Sastre-Santos, Á.; Ortí, E.; Gierschner J. A Deep-Red-Emitting Perylenediimide−Iridium-Complex Dyad: Following the Photophysical Deactivation Pathways. *J. Phys. Chem. C* **2009**, *113*, 44, 19292-19297; e) Martre, A.; Laguitton-Pasquier, H.; Deronzier, A.; Harriman, A. Preparation and Properties of a Soluble Polypyrrole−Polypyridyl−Ruthenium(II)−Viologen Dyad. *J. Phys. Chem. B* **2003**, *107*, 12, 2684-2692.

[11] Chen, Y.; El-Khouly, M. E.; Sasaki, M.; Araki, Y.; Ito, O. Synthesis of the Axially Substituted Titanium Pc-C60 Dyad with a Convenient Method. *Org. Lett.* **2005**, *8*, 1613–1616.

[12] Nishikawa, H.; Kojima, S.; Kodama, T.; Ikemoto, I.; Suzuki, S.; Kikuchi, K.; Fujitsuka, M.; Luo, H.; Araki, Y.; Ito, O.; Photophysical Study of New Methanofullerene-TTF Dyads: An Obvious Intramolecular Charge Transfer in the Ground States. *J. Phys. Chem. A* **2004**, *108*, 1881-1890

[13] Leroy-Lhez, S.; Perrin, L.; Baffreau, J.; Hudhomme, P. Perylenediimide derivatives in new donor–acceptor dyads. *C. R. Acad. Chim.* **2006**, *9*, 240-246.

[14] Tsujimoto, K.; Ogasawara, R.; Nakagawa, T.; Fujiwara, H. Photofunctional Conductors Based on TTF-BODIPY Dyads Bearing p-Phenylene and p-Phenylenevinylene Spacers. *Eur. J. Inorg. Chem.* **2014**, *24*, 3960-3972.

[15] Jia, H.; Schmid, B.; Liu, S.-X.; Jaggi, M.; Monbaron, P.; Bhosale , S. V.; Rivadehi,S.; Langford, S. J.; Sanguinet, L.; Levillain, E.; El-Khouly, M. E.; Morita, Y.; Fukuzumi, S.; Decurtins, S. Tetrathiafulvalene-Fused Porphyrins via Quinoxaline Linkers: Symmetric and Asymmetric Donor–Acceptor Systems. *Chem. Phys. Chem.* **2012**, *13*, 3370 – 3382.

[16] Zhang, G.; Zhang, D.; Zhao, X.; Ai, X.; Zhang, J.; Zhu, D. Assembly of a Tetrathiafulvalene–Anthracene Dyad on the Surfaces of Gold Nanoparticles: Tuning the Excited-State Properties of the Anthracene Unit in the Dyad. *Chem. Eur. J.* **2006**, *12*, 1067 – 1073.

[17] Keniley, L. K.; Dupont, N.; Ray, L.; Ding, J.; Kovnir, K. Hoyt, J. M.; Hauser, A.; Shatruk, M. Complexes with Redox-Active Ligands: Synthesis, Structure, and Electrochemical and Photophysical Behavior of the Ru(II) Complex with TTF-Annulated Phenanthroline. *Inorg. Chem.* **2013**, *52*, 8040−8052.

[18] Weekes, D. M.; Baradel, N.; Kyritsakas, N.; Mobian, P.; Henry, M. Rational Synthesis of a Family of Neutral Monomeric Heteroleptic Titanium Complexes Based on an Octahedral TiO_4N_2 Motif. *Eur. J. Inorg. Chem.* **2012**, *34*, 5701-5713.

[19] Keniley, L. K.; Ray, L .; Kovnir, K.; Dellinger, L. A. ; Hoyt, J. M.; Shatruk, M. TTF-Annulated Phenanthroline and Unexpected Oxidative Cleavage of the C═C Bond in Its Ruthenium(II) Complex. *Inorg. Chem.* **2010**, *49*, 1307-1309.

[20] Diebold, C.; Mobian, P.; Huguenard, C.; Allouche, L.; Henry, M. Synthesis and characterization of a monomeric octahedral C2-symmetric titanium complex bearing two 3,3'-diphenyl-2,2'-biphenol ligands. *Dalton Trans.* **2009**, 10178–10180.

[21] Felder, D.; Nierengarten, H.; Gisselbrecht, J.-P.; Boudon, C.; Leize, E.; Nicoud, J.-F.; Gross, M.; Van Dorsselaer, A.; Nierengarten, J.-F. Fullerodendrons: synthesis, electrochemistry and reduction in the electrospray source for mass spectrometry analysis. *New J. Chem.* **2000**, *24*, 687–695.

[22] a) Sonström, A.; Boldrini, B.; Werner, D.; Maichle-Mössmer, C.; Rebner, K.; Casu, M. B.; Anwander, R. Titanium(IV) Surface Complexes Bearing Chelating Catecholato Ligands for Enhanced Band-Gap Reduction. *Inorg. Chem.* **2023**, *62*, 715-729; b) Senouci, H.; Millet, B.; Volkringer, C.; Huguenard, C.; Taulelle, F.; Henry, M. Full spectroscopic characterization of an hydrolytically stable and colored Ti(IV)-precursor in solution. *C. R. Chimie* **2010**, *13*, 69-96.

[23] Grimme, S; Hansen, A; Brandenburg, J. G.; Bannwarth, C. Dispersion-Corrected Mean-Field Electronic Structure Methods. *Chem. Rev.* **2016**, *116*, 5105-5154.

[24] Weigend, F.; Ahlrichs, R.; Balanced basis sets of split valence, triple zeta valence and quadruple zeta valence quality for H to Rn: Design and assessment of accuracy. *Phys. Chem. Chem. Phys.*, **2005**, *7*, 3297–3305.

[25] Scalmani, G.; Frisch, M. J.; Continuous surface charge polarizable continuum models of solvation. I. General formalism, *J. Chem. Phys.* **2010**, *132*, 114110.

[26] Gaussian 09, Revision D.01, Frisch, M. J.; Trucks, G. W.; Schlegel, H. B.; Scuseria, G. E.; Robb, M. A.; Cheeseman, J. R.; Scalmani, G.; Barone, V.; Petersson, G. A.; Nakatsuji, H.; Li, X.; Caricato, M.; Marenich, A.; Bloino, J.; Janesko, B. G.; Gomperts, R.; Mennucci, B.; Hratchian, H. P.; Ortiz, J. V.; Izmaylov, A. F.; Sonnenberg, J. L.; Williams-Young, D.; Ding, F.; Lipparini, F.; Egidi, F.; Goings, J.; Peng, B.; Petrone, A.; Henderson, T.; Ranasinghe, D.; Zakrzewski, V.

G.; Gao, J.; Rega, N.; Zheng, G.; Liang, W.; Hada, M.; Ehara, M.; Toyota, K.; Fukuda, R.; Hasegawa, J.; Ishida, M.; Nakajima, T.; Honda, Y.; Kitao, O.; Nakai, H.; Vreven, T.; Throssell, K.; Montgomery, Jr., J. A.; Peralta, J. E.; Ogliaro, F.; Bearpark, M.; Heyd, J. J.; Brothers, E.; Kudin, K. N.; Staroverov, V. N.; Keith, T.; Kobayashi, R.; Normand, J.; Raghavachari, K.; Rendell, A.; Burant, J. C.; Iyengar, S. S.; Tomasi, J.; Cossi, M.; Millam, J. M.; Klene, M.; Adamo, C.; Cammi, R.; Ochterski, J. W.; Martin, R. L.; Morokuma, K.; Farkas, O.; Foresman, J. B.; Fox, D. J. Gaussian, Inc., Wallingford CT, **2016**.

[27] Scarpi-Luttenauer, M.; Geminiani, L.; Lebrun, P.; Kyritsakas, N.; Chaumont, A.; Henry, M.; Mobian, P. Bent 1,10-Phenanthroline Ligands within Octahedral Complexes Constructed around a TiO_4N_2 Core. *Inorg. Chem.* **2020**, *59*, 12005–12016.

[28] Laguta, V. V.; Glinchuk, M. D.; Kuzian, R. O.; Nokhrin, S. N.; Bykov, I. P.; Rosa, J.; Jastrabik, L; Karkut, M. G. The photoinduced Ti^{3+} centre in $SrTiO_3$. *J. Phys.: Condens. Matter* **2002**, 14, 13813–13825.

[29] a) Halpin, Y.; Schulz, M.; Brooks, A. C.; Browne, W. R.; Wallis, J. D.; Gonzalez, L.; Day, P.; Vos, J. G. Electrochemistry and time dependent DFT study of a (vinylenedithio)-TTF derivative in different oxidation states. *Electrochim. Acta* **2013**, *100*, 188. b) Andreu, R.; Garín, J.; Orduna, J. Electronic absorption spectra of closed and open-shell tetrathiafulvalenes: the first time-dependent density-functional study. *Tetrahedron* **2001**, *57*, 7883. c) Boulmier, A.; Vacher, A.; Zang, D.; Yang, S.; Saad, A.; Marrot, J.; Oms, O.; Mialane, P.; Ledoux, I.; Ruhlmann, L.; Lorcy, D.; Dolbecq, A. Anderson-Type Polyoxometalates Functionalized by Tetrathiafulvalene Groups: Synthesis, Electrochemical Studies, and NLO Properties. *Inorg. Chem.* **2018**, 57, 3742-3752.

[30] a) Wang, W.-K.; Chen, Y.-Y.; Wang, H.; Zhang, D.-W.; Liu, Y.; Li, Z.-T. Tetrathiafulvalene-Based Macrocycles Formed by Radical Cation Dimerization: The Role of Intramolecular Hydrogen Bonding and Solvent. *Chem. Asian J.* **2014**, 9, 1039-1044. b) Yoshizawa, M.; Kumazawa, K.; Fujita, M. Room-Temperature and Solution-State Observation of the Mixed-Valence Cation Radical Dimer of Tetrathiafulvalene, $[(TTF)2]^{+\bullet}$ within a Self-Assembled Cage. *J. Am. Chem. Soc.* **2005**, *127*, 13456-13457. c) Ziganshina, A. Y.; Ko, Y. H.; Jeon, W. S.; Kim, K. Stable π-dimer of a tetrathiafulvalene cation radical encapsulated in the cavity of cucurbit[8]uril. *Chem. Commun.* **2004**, 806-807.

[31] Bandyopadhyay, B.; Harriman, A. Photoreduction of 1,10-phenanthroline. *J. Chem. Soc., Faraday Trans.* **1977**, *73*, 663-674.

[30] Sheldrick, G. M., **1996**, SADABS, University of Göttingen, Germany.

[31] Sheldrick, G. M., Crystal structure refinement with SHELXL, *Acta Cryst. C* **2015**, *71*, 3-8.

[32] Krejcík, M.; Danek, M.; Hartl, F.; Simple construction of an infrared optically transparent thin-layer electrochemical cell: Applications to the redox reactions of ferrocene, $Mn_2(CO)_{10}$ and $Mn(CO)_3$(3,5-di-*t*-butyl-catecholate)$^-$. *J. Electroanal. Chem.* **1991**, *317*, 179-187.

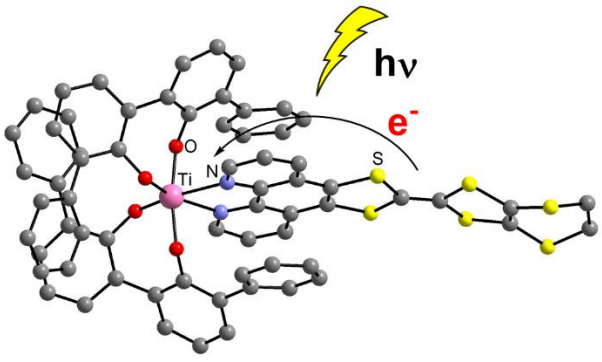

Synopsis

A dyad containing a Ti(IV) centre coordinated by a 1,10-phenanthroline ligand containing a TTF fragment was prepared. Upon visible light excitation, a charge separated state is reached, where the TTF unit is oxidized and the Ti-phenanthroline unit is reduced.